Chemical Physics Letters 651 (2016) 268–273

Contents lists available at ScienceDirect

Chemical Physics Letters

journal homepage: www.elsevier.com/locate/cplett

A PW91-like exchange with a simple analytical form

Juan C. Pacheco-Kato[a], Jorge M. del Campo[b], José L. Gázquez[c], S.B. Trickey[d], Alberto Vela[e,*]

[a] Departamento de Química, Universidad de Guanajuato, Noria Alta s/n, Colonia Noria Alta, 36050 Guanajuato, GTO, Mexico
[b] Departamento de Física y Química Teórica, Facultad de Química, Universidad Nacional Autónoma de México, México D.F. 04510, Mexico
[c] Departamento de Química, Universidad Autónoma Metropolitana-Iztapalapa, Av. San Rafael Atlixco 186, México D.F. 09340, Mexico
[d] Quantum Theory Project, Dept. of Physics and Dept. of Chemistry, University of Florida, P.O. Box 118435, Gainesville, FL 32611-8435, USA
[e] Departamento de Química, Cinvestav, Av. IPN 2508, Colonia San Pedro Zacatenco 07360, México D.F. 07360, Mexico

ARTICLE INFO

Article history:
Received 10 December 2015
In final form 10 March 2016
Available online 12 April 2016

ABSTRACT

A pair of families of generalized gradient approximation (GGA) exchange functionals is presented. The aim is to simplify the PW91 enhancement factor considerably, yet retain its shape, not degrade its performance and, within those confines, improve on it. The functionals are constructed non-empirically by taking as kernels the PBE and RPBE analytic forms and adding a Gaussian tail to comply with the asymptotic reduced-gradient constraint from non-uniform scaling. Standard heats of formation are considerably improved by the functionals compared to PBE. Globally, the new functionals exhibit much better balance in predicting thermodynamic and kinetic properties than any competing non-empirical GGA.

1. Introduction

Nowadays, the method of choice to study the electronic structure of molecules, clusters, surfaces, and solids, especially when the number of electrons is large, is the Kohn–Sham (KS) approach within density functional theory (DFT) [1–3]. In the KS formulation, the exchange-correlation (XC) energy functional is an elusive entity that has received much attention in the last 50 years. Among the many approximations that have been proposed, those derived via non-empirical constraint satisfaction are particularly appealing, partly because the non-empirical parameterization enhances confidence in the applicability of such XC functionals to a broad range of situations and partly because the enforcement of competing constraints provides insight into the role played by those constraints in providing predictive capability for practical KS theory. The constraint-based school, introduced and explored by Perdew and coworkers [4–6] has proposed a series of XC-functionals belonging to different rungs of the Jacob's ladder classification scheme [7]. It appears that to achieve needed accuracy in predicted properties related to the electronic structure of matter it often is necessary to climb the ladder beyond the second rung (which corresponds to the generalized gradient approximation, GGA). However, if one is interested in large systems or in properties requiring many evaluations, such as those along an ab initio molecular dynamics trajectory, then doing the calculations with a GGA is highly desirable because of computational costs. Therefore, there remains value in seeking further improvement in GGA functionals.

Among the best known non-empirical GGA functionals are PW91 [4] and PBE [5], in the latter case with its revisions, revPBE [8] and RPBE [9]. Unfortunately, the errors produced by these GGAs in thermodynamic and kinetic properties on standard test sets are far from chemical accuracy (mean absolute energetic errors less than 1 kcal/mol). Moreover, they are unbalanced in the sense that the errors made in predicting thermodynamic properties are markedly different from those for kinetic properties. Another feature to be noted is that the analytical form of PW91 is cumbersome and can lead to numerical instabilities. In fact, this was one of the motivations for Perdew, Burke and Ernzherhof [5] to propose PBE. One of the conditions satisfied by PW91 is the asymptotic behavior of the exchange enhancement factor in the limit of large dimensionless gradient [10], a constraint not satisfied by the majority of non-empirical GGAs. We have explored this issue in other contexts [11,12]. The original form of the limit is an inequality. Subsequently it has been argued that the limit is a strict equality [13–16] which imposes a specific decay upon the exchange enhancement factor. That stricter behavior is not satisfied by PW91.

In this Letter we present and test a family of non-empirical GGA exchange functionals (X-functionals) that incorporate the large dimensionless gradient constraint by having the functionals reproduce, as closely as reasonably possible, the shape of the PW91

* Corresponding author.
E-mail address: avela@cinvestav.mx (A. Vela).

http://dx.doi.org/10.1016/j.cplett.2016.03.028
0009-2614/

exchange enhancement factor but with a simpler analytical form. It therefore is consistent to enforce the large dimensionless gradient constraint in its original form [10]. Thus, in what follows, when we say that a functional complies with the large dimensionless exchange gradient asymptotic limit, it is in the broader, original sense. One of our XC energy functionals performs substantially better on atomization errors than previous GGAs, does not sacrifice other GGA performance relative to PBE, and is more balanced (in the thermodynamic vs. kinetic sense) than other non-empirical GGA functionals. Indeed, we now have a GGA that is within the range of performance on standard tests of some older meta-GGAs and not too far off from B3LYP [17–21], a popular hybrid functional.

A GGA exchange functional typically is written in terms of an enhancement factor, F_X, with respect to local exchange as

$$\begin{aligned} E_X[\rho] &= \int dr \quad \rho(r) \quad \varepsilon_X^{LDA}(\rho) \quad F_X(s), \\ \varepsilon_X^{LDA}(\rho) &= C_X \quad \rho^{1/3}(r), \\ C_X &= -\frac{3}{4}\left(\frac{3}{\pi}\right)^{1/3}, \end{aligned} \tag{1}$$

where the dimensionless gradient s is given by

$$s(\mathbf{r}) = \frac{|\nabla\rho|}{2(3\pi^2)^{1/3}\rho^{4/3}}. \tag{2}$$

The non-empirical PW91 exchange was designed considering the following conditions: (a) it is an analytical fit to the numerical values of exchange energies of a system with slowly varying density, using real space cutoffs to enforce constraints on the exchange hole that eliminate the spurious long-range behavior of the second-order density gradient expansion; (b) it satisfies a tight local Lieb–Oxford (LO) [22] bound of 1.641 and, (c) it complies with the asymptotic behavior of the enhancement factor in the limit of large s that results from non-uniform scaling conditions [10]. However, in the words of Perdew, Burke, and Ernzerhof [5], the PW91 enhancement factor is complicated, non-transparent, and overparametrized. It has the analytical form [4]

$$F_X^{PW91}(s) = \frac{1 + 0.19645s\,\sinh^{-1}(7.7956s) + (0.2743 - 0.1508\,e^{-100s^2})s^2}{1 + 0.19645s\,\sinh^{-1}(7.7956s) + 0.004s^4}. \tag{3}$$

As mentioned above, PBE was introduced with the intention of simplifying the complicated PW91 form while keeping its predictive capabilities. The much simpler PBE enhancement factor is [5]

$$F_X^{PBE}(s) = 1 + \kappa - \frac{\kappa}{1 + ((\mu s^2)/\kappa)}, \tag{4}$$

where μ and κ are non-empirical parameters. Widely used to study molecular and extended systems, PBE provides reasonably good prediction of properties such as ionization potentials (IP), electron affinities (EA), and bond lengths (BL), but is still far from chemical accuracy for atomization energies or heats of formation.

The simple analytical form of the PBE enhancement factor led to many proposed modifications aimed at improved performance. The two most obvious possibilities are to change the values of the parameters μ and κ. In the former case we find X-functionals like PBEsol [23], APBE [24], and PBEmol [25] that fix μ by imposing different constraints. Changing κ was the strategy followed in revPBE [8]. In doing so, the value of the local LO-bound was increased. Another route to modify PBE is to keep its minimalistic philosophy but explore different analytical forms for the exchange enhancement factor. Along this line we can mention the X-functionals RPBE [9] VMT [26], and VT{m,n} [11]. The RPBE enhancement factor, which will be relevant in the following sections, is [9]

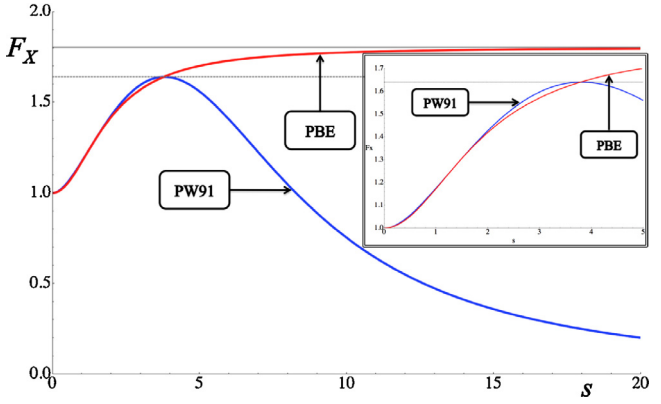

Figure 1. Exchange enhancement factors for PBE and PW91 in the interval $0 \le s \le 20$. The inset shows an expanded view on the interval $0 \le s \le 5$. The solid and dashed gray horizontal lines are the values of the local Lieb-Oxford bound used in PBE and PW91, respectively.

$$F_X^{RPBE}(s) = 1 + \kappa\left(1 - e^{-((\mu s^2)/\kappa)}\right). \tag{5}$$

2. Mimicking PW91

The most important difference between PW91 and PBE is their asymptotic behavior with respect to s, as can be seen clearly in Figure 1. Both functionals go almost parallel up to s values around 3 (see inset in Figure 1). Then, in the region $3 \le s \le 5$, PW91 reaches a maximum of 1.641 while PBE continues growing and, finally for large gradients, $s > 5$, PW91 monotonically decreases to its asymptotic value of zero, while PBE approaches the constant asymptote corresponding to the local LO bound. This happens because PW91 was designed to satisfy the constraint [10]

$$\lim_{s\to\infty} s^{1/2} F_X(s) < \infty, \tag{6}$$

that comes from 1-D and 2-D non-uniform scaling conditions. This inequality requires $F_X(s)$ to decay to zero at least as fast as $s^{-1/2}$. As mentioned above, recently it has been argued that the large dimensionless gradient constraint is a strict equality which requires decay of the exchange enhancement factor as $s^{-1/2}$ [16]. Here we enforce the original form [10] since our motivation is to reproduce and, if possible, improve upon, PW91 X, which decays as s^{-2}, with a simplified form. We note, however, that no GGA X functional can satisfy all known constraints. The choice to enforce Eq. (6) has the quite specific consequence that the large r behavior of the exchange potential will be incorrect. See Ref. [27] for detailed investigation of this issue and references therein.

To incorporate the large gradient constraint, Eq. (6), we employ ideas similar to those we used recently in tailoring the X-functional PBE-LS [12] but with the design strategy of mimicking PW91 as closely as possible with a simple enhancement factor. Therefore, we propose adding to the PBE and RPBE exchange enhancement factors the GAUSSIAN tail $-(\kappa+1)e^{-\alpha s^2}$, thus producing two GGA exchange functionals that we denote as lsPBE and lsRPBE, respectively. Note that this tail also decays more rapidly than is required by Eq. (6). The new enhancement factors are

$$F_X^{lsPBE/lsRPBE}(s) = F_X^{PBE/RPBE}(s) - (\kappa+1)(1 - e^{-\alpha s^2}). \tag{7}$$

To fix the parameters μ, κ and α we proceed as follows. By expanding Eq. (7) in a power series in s we obtain

$$F_X^{lsPBE/lsRPBE}(s) = 1 + (\mu - \alpha - \alpha\kappa)s^2 + O(s^4). \tag{8}$$

Clearly, the coefficient of the quadratic term depends on the three parameters defining the functional. Also, note that this coefficient is the same for both X-functionals. Considering that the value of this coefficient previously has been established by several non-empirical considerations, we enforce the requirement that

$$\mu_X = \mu - \alpha - \alpha\kappa, \tag{9}$$

where μ_X is any one of the following non-empirical choices:

(a) The original value used in PBE, $\mu_X = \mu_{PBE} = 0.219516$ [5].
(b) The value obtained from the gradient expansion approximation $\mu_X = \mu_{GEA} = 10/81$ [28].
(c) The value obtained from the asymptotic expansion of the semi-classical approximation, called the modified gradient expansion approximation (MGEA), $\mu_X = \mu_{MGEA} = 0.26$. This value is used in the APBE functional [24].
(d) The value deduced from atomic hydrogen as used in PBEmol, $\mu_X = \mu_{mol} = 0.27583$ [25].

To distinguish the exchange functionals proposed here, to each of the family labels lsPBE and lsRPBE, we add the suffixes NONE, sol, MGEA, and mol to indicate the corresponding μ_X value. To clarify, for the PBE family we will use the labels lsPBE, lsPBEsol, lsPBEMGEA and lsPBEmol, and likewise with lsRPBE.

With the purpose of keeping the forms of the proposed functionals close to the PBE and RPBE kernels, we will use the original value for κ (0.804) used in PBE and RPBE. We determine α, the variable that controls the enhancement factor decay in the large-s region, by requiring that the enhancement factor maximum (the local LO bound) be equal to the PW91 value, 1.641. This design choice is motivated by the goal of mimicking PW91-exchange. Thus, by numerical solution of

$$\frac{dF_X^{lsPBE/lsRPBE}(s_{MAX})}{ds} = 0 \tag{10}$$

$$F_X^{lsPBE/lsRPBE}(s_{MAX}) = 1.641, \tag{11}$$

and use of Eq. (9), we obtain the values of α and μ corresponding to each value of μ_X mentioned in the previous paragraph. The parameters for each functional are reported in Table 1.

The exchange enhancement factors corresponding to the lsRPBE family are compared with PW91 in Figure 2. The salient feature to be noted is that this new family resembles PW91 much better than any of the lsPBE family (see Figure S1). The inset in Figure 2 shows that when μ_X increases, the lsRPBE exchange functionals increase faster toward their maxima, then (see Figure 2) decrease faster toward the asymptotic zero for large s.

To summarize the differences in the behaviors of the original functionals (PBE and RPBE) with the exchange GGAs that satisfy the large gradient constraint (lsPBE and lsRPBE), Figure 3 depicts the four possibilities corresponding to $\mu_X = \mu_{PBE}$ and, for comparison, the PW91 enhancement factor. Clearly, all the exchange functionals have very similar behavior in the interval $0 \le s \le 1$. By design, the kernel functionals (PBE and RPBE) saturate to the local Lieb–Oxford bound in the limit $s \to \infty$. The modified functionals

Table 1
Values of α and μ for the lsPBE and lsRPBE families of GGA exchange functionals. Rows are ordered by increasing value of μ_X.

μ_X	lsPBE		lsRPBE	
	α	μ	α	μ
μ_{GEA}	0.00081642	0.1249296	0.00382940	0.1303650
μ_{PBE}	0.00145165	0.2221328	0.00680892	0.2317973
μ_{MGEA}	0.00171938	0.2631018	0.00806472	0.2745488
μ_{mol}	0.00182407	0.2791206	0.00855574	0.2912645

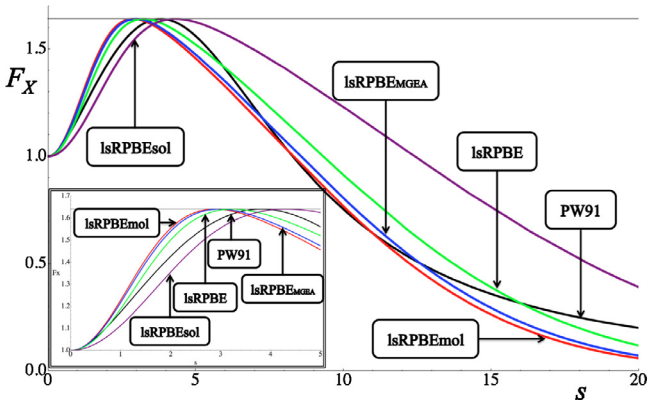

Figure 2. As in Figure 1 for the lsRPBE family and PW91. The solid gray horizontal line is the local Lieb-Oxford bound used in PW91.

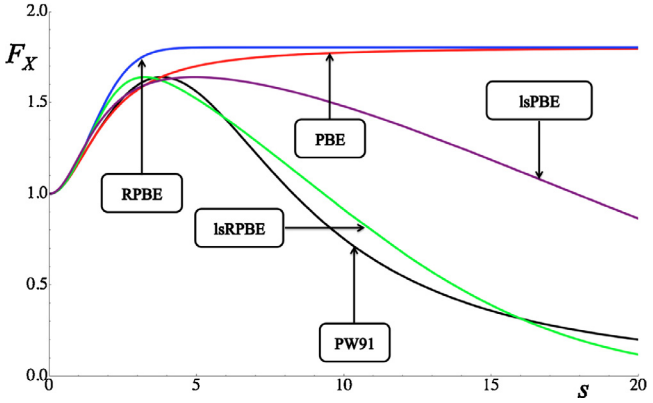

Figure 3. Comparison of exchange enhancement factors for the functionals identified by the labels.

(lsPBE and lsRPBE) by design decay to zero, with lsRPBE having the closest shape to PW91, but with a much simple analytical form. The question then is the consequences of these differences.

To perform the validation calculations, one must choose a correlation functional. In what follows, we combined the GGA exchange functionals with the GGA correlation functionals PBE [5], PW91 [4], and LYP [18,29]. In the first case, the parameter β that appears in the correlation function was fixed by enforcing cancelation of the quadratic terms in the gradients that appear in exchange and correlation, a condition that leads to the relation

$$\beta = \frac{3\mu_X}{\pi^2}. \tag{12}$$

3. Methodology and test sets

The lsPBE and lsRPBE families of GGA exchange functionals were implemented in NWChem [30]. The obligatory reference non-empirical GGA functionals are PBE, RPBE, and PW91, for which results also are reported. All the properties calculated in this work were obtained from self-consistent calculations of the systems in the test sets according to standard protocols for each set.

Specifically, we calculated the standard heats of formation of the G3 test set (223 molecules) [31,32]. Following Curtiss et al. [33], all molecular geometries were optimized with B3LYP [17,18,19,20,21] using the 6-31G(2df,p) basis set [34]. The harmonic frequencies were scaled by 0.9854. Standard heats of formation were evaluated by single-point calculations with the corresponding functional and the Def2-TZVPP basis set [35]. Ionization potentials (IP) and electron affinities (EA) were computed for the IP13/3 and EA13/3 datasets [36,37]. For both, the calculations were done

adiabatically using geometries from Ref. [32] with a 6-31++G(d,p) basis set. The proton affinities (PA) were calculated with the geometries obtained from MP2(full)/6-31G(2df,p) calculations of the anions and neutral species, with geometries taken from the Computational Thermochemistry database [38] and the 6-31++G(d,p) basis sets. For performance appraisal on weakly interacting systems, we chose 31 systems divided in different test sets comprised of six hydrogen-bonded dimers (HB6/04) [39], seven involving charge transfer (CT7/04) [39], six dipole interaction complexes (DI6/04) [39], seven nominally dispersion-interacting systems (WI7/05) [40], and five π–π stacking complexes (PPS5/05) [40]. The binding energies were obtained from single-point calculations using the 6-31++G(d,p) basis set at geometries taken from Ref. [41]. Energy barrier heights also were calculated for 38 hydrogen transition reactions (HTBH38/04) and 38 non-hydrogen transition reactions (NHTBH83/04), as proposed by Zhao and Truhlar [40,42,43]. For each reaction, single-point calculations of the reactants, products, and transition states were done with the Def2-TZVPP basis set and the QCISD/MG3 geometries, available from Ref. [41]. Bond lengths also were calculated for the 96 small molecules in the T-96R database proposed by Staroverov et al. [32]. All of those calculations were done with the Def2-TZVPP basis set. Finally, harmonic vibrational frequencies were evaluated for the T-82F database [32], using the Def2-TZVPP basis set.

4. Results

To set some context for what constitutes improvement in the performance of the functionals, the calculated mean absolute deviations (MADs) for the standard heats of formation obtained from the non-empirical GGA functionals PBE, RBE and PW91 for the G3 set are 21.21, 13.0, and 22.61 kcal/mol, respectively. The first two exchange functionals were combined with PBE correlation, while PW91 was used with its own correlation functional. The MAD results are in complete agreement with published validations of these functionals. For this property, PBE and PW91 perform very similarly, while RPBE improves with a MAD reduction of about 40%.

For the PW91-like functionals, MADs for the G3 standard heats of formation reported in Table 2 show the following trends. For the lsPBE family, irrespective of the correlation functional used, the MAD of this property decreases as the value of μ_X increases. For this exchange, the correlation that provides the smallest MAD in heat of formation is LYP, i.e., the XC-functional lsPBEmol-LYP. The trend obtained with the lsRPBE family shows that for all the correlation functionals considered, the smallest MADs are achieved when using $\mu_X = \mu_{PBE}$. In this family, the non-empirical correlation functionals PBE and PW91 have the smallest MADs of around 7.8 kcal/mol. Thus, the best functional among this family is lsRBE-PW91. It is gratifying to find that this X-functional, which is related to PW91, is the one with the smallest MAD. It provides a 67% decrease in the MAD of the standard heats of formation with respect to the original PW91. It is also worth noting that for the lsPBE family, independently of the value of μ_X, the LYP C-functional provides the smallest MADs, a trend that is not seen in the lsRPBE family. Thus, one can conclude that the X-functionals of each family with the best performance in predicting standard heats of formation are lsPBEmol and lsRPBE. The complete set of results for all the functionals considered can be found in the Supplementary Material.

Table 2
MADs for the standard heats of formation of the G3 set for the lsPBE and lsRPBE families of functionals combined with the PBE, PW91, and LYP correlation functionals. Rows are ordered by increasing value of μ_X. All data are in kcal/mol.

μ_X	X	lsPBE			lsRPBE		
	C	PBE	PW91	LYP	PBE	PW91	LYP
sol		60.15	53.55	43.85	46.16	39.62	29.93
PBE		24.00	23.88	14.77	7.94	7.51	12.56
MGEA		12.71	15.65	8.29	15.94	12.13	20.36
mol		10.68	12.94	7.62	20.09	15.07	23.46

On the basis of the MAD results for the G3 heats of formation, and for the sake of brevity, we present complete results for the remaining validation only for the X-functionals lsPBEmol and lsRPBE. Table 3 shows the results for all the properties described in the previous section. To have some context for comparison, results for PBE, RPBE, and PW91 are included. Similarly, results are provided for the non-empirical GGAs developed in our group that satisfy the large-s constraint, namely, VT{8,4} [11] and PBE-LS [12]. For both lsPBE and lsRPBE, results are shown in combination with PBE, PW91, and LYP correlation. Results for lsPBEmol combined with PBEmol correlation (PBE correlation with the parameter β fixed according to Eq. (12) using $\mu_X = \mu_{mol}$) also are given.

For the standard heats of formation of the G3 test set (row labeled G3 in Table 3) we conclude as before that lsRPBE-PW91 is the functional with the smallest MAD. It is also interesting to note that the non-empirical X-functional VT{8,4}, that satisfies the large-s constraint but with a different analytical decaying function, has a smaller MAD for the standard heats of formation than two of the three non-empirical lsPBEmol XC combinations, but does not outperform the non-empirical lsRPBE functional for the same correlation functionals. This pattern may be a result of the deliberate effort in VT{8,4} to provide a plateau at $F_s \approx 1$ for mid-range s values. Or it may have something to do with the use of GAUSSIANS in lsRPBE to describe the short- and large-s behavior of the enhancement factor, since the kernel also is built with Gaussians. For the ionization potentials (row labeled IP in Table 3), RPBE shows the best performance, followed very closely by VT{8,4}-PBE and lsRPBE-PBE, while the lsPBEmol family shows the largest MADs in this property. The electron affinities (row labeled EA in Table 3) exhibit trends similar to the IPs: VT{8,4}, RPBE, and lsRPBE-PBE, in that order, provide the smallest MADs for this property. The MADs are very close to each other (within 0.11 kcal/mol). For the proton affinities (row labeled PA in Table 3), the MAD of lsRPBE-PBE is only 0.17 kcal/mol larger than that of VT{8,4}.

PW91 is the GGA X functional with the smallest MADs for the bond lengths and harmonic frequencies (rows labeled BL and Freq, respectively, in Table 3). In this case, the lsPBEmol family provides MADs that are close to PW91. However it should be noted that both families, lsPBE and lsRPBE, are within 2 pm and 10 cm^{-1} away from PW91, values that are very well within the range of typical experimental error.

The description of weak interactions (row labeled WI in Table 3) is very similar for all the GGA functionals considered here. The MADs range from 1.52 kcal/mol (RPBE, lsRPBE-PBE and lsRPBE-PW91 have the same MAD) to 1.98 kcal/mol (lsPBEmol-LYP), with an average of 1.65 kcal/mol and standard deviation of 0.15 kcal/mol. Thus, the inclusion of the large-s behavior and the modification of the Lieb–Oxford bound do not alter significantly the description of WIs with respect to the kernels PBE and RPBE.

The last properties to be analyzed are the reaction barrier heights. Simple comparison of MADs misses a chemically important point. A more insightful analysis proceeds by taking the difference between the MAD corresponding to the standard heats of formation (G3 set) and the average of the four MADs reported for each functional, (NHBH-f/r and HBH-f/r sets). This difference should measure the balance in predicting energy differences associated with valleys in the potential energy surface (products minus reactants) and those involving saddle points (transition states minus reactants or products). This analysis is reported in Table 4. Interestingly, one sees that the non-empirical GGA functionals that were designed to satisfy the large s asymptotic behavior are the ones having the smallest differences, i.e., they are the ones that are best balanced

Table 3
MADs for the heats of formation (G3), ionization potentials (IP), electron affinities (EA), proton affinities (PA), bond lengths (BL), frequencies (Freq), weak interacting systems (WI), and barrier heights for non-hydrogen transfer reactions (NHBH-f/r) and for hydrogen transfer reactions (HBHf/r). All energy data are in kcal/mol, distances in Å, and frequencies in cm^{-1}.

Property	X C	PBE PBE	RPBE PBE	PW91 PW91	VT{8,4} PBE	PBE-LS PBE	lsPBEmol PBEmol	lsPBEmol PW91	lsPBEmol LYP	lsRPBE PBE	lsRPBE PW91	lsRPBE LYP
G3		21.21	13.00	22.61	9.98	9.39	10.68	12.94	7.62	7.94	7.51	12.56
IP		3.47	3.00	4.47	3.26	3.65	4.11	5.81	5.12	3.31	3.57	4.02
EA		2.64	2.49	3.52	2.48	2.61	3.00	4.9	4.88	2.59	2.82	3.14
PA		1.39	1.31	1.31	1.07	1.23	1.57	1.67	1.98	1.24	1.28	1.52
BL		0.0179	0.0258	0.0164	0.0208	0.0216	0.0187	0.0183	0.025	0.0233	0.0231	0.028
Freq		43.3	50.67	37.76	49.23	45.74	40.55	38.74	57.65	46.25	44.83	64.96
WI		1.64	1.52	1.8	1.53	1.49	1.57	1.67	1.98	1.52	1.52	1.73
NHBH-f		10.38	9.03	10.7	9.79	7.26	9.97	10.48	11.67	9.69	9.74	10.92
NHBH-r		9.96	8.81	10.2	9.46	7.77	9.81	10.14	11.17	9.38	9.42	10.45
HBH-f		9.49	6.5	9.78	8.23	9.45	8.24	8.6	8.91	7.62	7.54	7.81
HBH-r		9.72	7.04	9.96	8.59	9.31	8.69	8.91	9.04	8.12	8.01	8.11

Table 4
Rows labeled as Avg. and Std. dev. are the mean and standard deviations, respectively, of the MADs for the four classes of reaction barrier heights reported in Table 3. The row labeled Difference is the difference between the MAD corresponding to the standard heat of formation of the G3 set and the average of the barrier heights for the functionals shown on the top of each column. All these quantities are in kcal/mol.

Property	X C	PBE PBE	RPBE PBE	PW91 PW91	VT{8,4} PBE	PBE-LS PBE	lsPBEmol PBEmol	lsPBEmol PW91	lsPBEmol LYP	lsRPBE PBE	lsRPBE PW91	lsRPBE LYP
Avg.		9.89	7.85	10.16	9.02	8.45	9.18	9.53	10.20	8.70	8.68	9.32
Std. dev.		0.33	1.09	0.35	0.63	0.95	0.73	0.79	1.24	0.86	0.92	1.38
Difference		11.32	5.16	12.45	0.96	0.94	1.50	3.41	−2.58	−0.76	−1.17	3.24

Table 5
Least MAD for each data set compared to MAD for ls-RPBE-PW91.

Data set	Least MAD	(functional)	lsRPBE-PW91 MAD	Difference (%)
G3	7.51	(lsRPBE-PW9)	7.51	0
IP	3.00	(RPBE-PBE)	3.57	19
EA	2.48	(VT{8,4})	2.82	14
PA	1.07	(VT{8,4})	1.28	20
BL	0.0164	(PW91)	0.0231	41
Freq	27.76	(PW91)	44.83	19
WI	1.49	(PBE-LS-PBE)	1.52	2
NHBH-f	7.26	(PBE-LS-PBE)	9.74	34
NHBH-r	7.77	(PBE-LS-PBE)	9.42	21
HBH-f	6.5	(RPBE-PBE)	7.54	18
HBH-r	7.04	(RPBE-PBE)	8.01	14

in describing thermodynamic and kinetic energy differences. We finally note that lsRPBE-PBE is the XC-functional with the smallest absolute difference, with lsRPBE-PW91 close to it. As was discussed in Section 2, it also is the X-functional enhancement factor with the greatest similarity to the PW91 enhancement factor.

By comparison with the least MAD for each of the eleven validation data sets, a complementary assessment of the balance provided by lsRPBE-PW91 emerges. The data in Table 5 show that lsRPBE-PW91 is dramatically superior to all other GGAs on heats of formation, while on eight of the other 10 data sets its MAD is 20% or less off of the *best* GGA MAD. Those best MADs come from four other GGAs. The largest deviation, 41%, from best MAD is for the bond length (BL). For it, the relevant point is that the actual MAD is a small fraction of a typical bond length, ≤2.5% or thereabouts. Thus lsRPBE-PW91 gives results that are consistently close to the best of a whole suite of other GGAs, another form of balanced performance.

A further general observation emerges from the results given in Table 5. Despite its popularity, PBE is not best on *any* of the standard molecular tests. Indeed, there are only three of the eleven tests for which a GGA that does not have an asymptotically vanishing X enhancement factor with respect to s nevertheless gives the best MAD. That GGA is RPBE on IP, HBH-f, and HBH-r. Clearly the non-uniform scaling asymptote helps shape the X enhancement factor beneficially in important regions of s.

As a final test we performed X-only calculations for the noble gas atoms to compare the exchange energies provided by the proposed families of GGA exchange functionals with Hartree–Fock values. The results reported in Table S14 show that PW91 is the GGA X-functional with the smallest deviation from HF but it is not better than the empirical GGA B88 (see Table III of reference [27]). The largest deviations obtained are for functionals with $\mu_X = \mu_{GEA}$, with a MAD of 2.5–2.6 hartree. The MADs for the functionals with $\mu_X = \mu_{PBE}$ and $\mu_X = \mu_{mol}$ are in the range of 0.4–0.8 hartree, values that are typical of other non-empirical GGA exchange functionals.

5. Conclusions

By mimicking the shape of PW91 exchange and a judicious choice of parametrization, we have succeed in achieving two goals. One is a simpler analytical form that resembles PW91. The other is to have the same or better performance than PW91. This latter goal is substantially achieved by lsRPBE-PW91, which provides a dramatic improvement on heat of formation, IP, and EA MADs. This validation shows that addition of the asymptotic tail to RPBE causes little or no degradation compared to PW91 or PBE. Instead it yields a functional that is well-balanced in comparison with the best GGA performance on various standard validation tests. The result is a functional whose MAD for atomization energies is 35% of the PBE result, is almost as simple, and loses little or nothing for that large gain. Indeed, lsRPBE exchange combined with PW91 correlation substantially outperforms our previous best functional for molecules, PBE-LS. Moreover, the lsRPBE-PW91 combination provides excellent balance in predicting thermodynamic and kinetic properties, without sacrifice of either category for the benefit of the other.

Acknowledgements

AV was partially supported by Conacyt (project 128369). JCPK thanks Conacyt for financial support (project 128369). We thank CGSTIC-Cinvestav for providing computing time in the 'Xiuhcoatl Hybrid Supercomputing Cluster'. SBT was supported in part by U.S. NSF grant DMR-1515307. JMC acknowledges support provided by

DGAPA–UNAM Grant No. IA102114. JLG thanks Conacyt for grants 155698 and 237045.

Appendix A. Supplementary data

Supplementary data associated with this article can be found, in the online version, at doi:10.1016/j.cplett.2016.03.028.

References

[1] W. Kohn, L.J. Sham, Phys. Rev. 140 (1965) 1133.
[2] E. Engel, R.M. Dreizler, Density Functional Theory: An Advanced Course, Springer-Verlag Berlin, Berlin, 2011, pp. 1.
[3] A.D. Becke, J. Chem. Phys. 140 (2014) 18.
[4] J.P. Perdew, J.A. Chevary, S.H. Vosko, K.A. Jackson, M.R. Pederson, D.J. Singh, C. Fiolhais, Phys. Rev. B 46 (1992) 6671.
[5] J.P. Perdew, K. Burke, M. Ernzerhof, Phys. Rev. Lett. 77 (1996) 3865.
[6] J.W. Sun, A. Ruzsinszky, J.P. Perdew, Phys. Rev. Lett. 115 (2015) 036402.
[7] J.P. Perdew, K. Schmidt, in: V.E. Van Doren, C. Van Alsenoy, P. Geerlings (Eds.), Density Functional Theory and its Application to Materials, AIP, New York, 2001.
[8] Y.K. Zhang, W. Pan, W.T. Yang, J. Chem. Phys. 107 (1997) 7921.
[9] B. Hammer, L.B. Hansen, J.K. Norskov, Phys. Rev. B 59 (1999) 7413.
[10] M. Levy, J.P. Perdew, Phys. Rev. B 48 (1993) 11638.
[11] A. Vela, J.C. Pacheco-Kato, J.L. Gázquez, J.M. del Campo, S.B. Trickey, J. Chem. Phys. 136 (2012) 144115.
[12] J.L. Gázquez, J.M. del Campo, S.B. Trickey, R.J. Alvarez-Mendez, A. Vela, in: S.K. Ghosh, P.K. Chattaraj (Eds.), Concepts and Methods in Modern Theoretical Chemistry, Taylor & Francis, 2013, p. 295.
[13] S. Kurth, J. Mol. Struct.-Theochem. 501 (2000) 189.
[14] L. Pollack, J.P. Perdew, J. Phys.-Condens. Matter 12 (2000) 1239.
[15] L. Chiodo, L.A. Constantin, E. Fabiano, F. Della Sala, Phys. Rev. Lett. 108 (2012) 126402.
[16] J.P. Perdew, A. Ruzsinszky, J.W. Sun, K. Burke, J. Chem. Phys. 140 (2014) 18a533.
[17] A.D. Becke, Phys. Rev. A 38 (1988) 3098.
[18] C.T. Lee, W.T. Yang, R.G. Parr, Phys. Rev. B 37 (1988) 785.
[19] A.D. Becke, J. Chem. Phys. 98 (1993) 5648.
[20] A.D. Becke, J. Chem. Phys. 98 (1993) 1372.
[21] P.J. Stephens, F.J. Devlin, C.F. Chabalowski, M.J. Frisch, J. Phys. Chem. 98 (1994) 11623.
[22] E.H. Lieb, S. Oxford, Int. J. Quantum Chem. 19 (1981) 427.
[23] J.P. Perdew, A. Ruzsinszky, G.I. Csonka, O.A. Vydrov, G.E. Scuseria, L.A. Constantin, X.L. Zhou, K. Burke, Phys. Rev. Lett. 100 (2008) 136406.
[24] L.A. Constantin, E. Fabiano, S. Laricchia, F. Della Sala, Phys. Rev. Lett. 106 (2011) 186406.
[25] J.M. del Campo, J.L. Gázquez, S.B. Trickey, A. Vela, J. Chem. Phys. 136 (2012) 104108.
[26] A. Vela, V. Medel, S.B. Trickey, J. Chem. Phys. 130 (2009) 244103.
[27] J. Carmona-Espindola, J.L. Gázquez, A. Vela, S.B. Trickey, J. Chem. Phys. 142 (2015) 054105.
[28] P.R. Antoniewicz, L. Kleinman, Phys. Rev. B 31 (1985) 6779.
[29] B. Miehlich, A. Savin, H. Stoll, H. Preuss, Chem. Phys. Lett. 157 (1989) 200.
[30] M. Valiev, E.J. Bylaska, N. Govind, K. Kowalski, T.P. Straatsma, H.J.J. Van Dam, D. Wang, J. Nieplocha, E. Apra, T.L. Windus, W. de Jong, Comput. Phys. Commun. 181 (2010) 1477.
[31] L.A. Curtiss, K. Raghavachari, P.C. Redfern, J.A. Pople, J. Chem. Phys. 112 (2000) 7374.
[32] V.N. Staroverov, G.E. Scuseria, J.M. Tao, J.P. Perdew, J. Chem. Phys. 119 (2003) 12129.
[33] L.A. Curtiss, K. Raghavachari, P.C. Redfern, J.A. Pople, J. Chem. Phys. 106 (1997) 1063.
[34] L.A. Curtiss, P.C. Redfern, V. Rassolov, G. Kedziora, J.A. Pople, J. Chem. Phys. 114 (2001) 9287.
[35] F. Weigend, R. Ahlrichs, PCCP 7 (2005) 3297.
[36] B.J. Lynch, Y. Zhao, D.G. Truhlar, J. Phys. Chem. A 107 (2003) 1384.
[37] Y. Zhao, D.G. Truhlar, J. Chem. Theory Comput. 2 (2006) 1009.
[38] L.A. Curtiss, K. Raghavachari, P.C. Redfern, V. Rassolov, J.A. Pople, J. Chem. Phys. 109 (1998) 7764.
[39] Y. Zhao, D.G. Truhlar, J. Chem. Theory Comput. 1 (2005) 415.
[40] Y. Zhao, D.G. Truhlar, J. Phys. Chem. A 109 (2005) 5656.
[41] B.J. Lynch, Y. Zhao, D.G. Truhlar, Minnesota Database Collection, 2006.
[42] Y. Zhao, N. Gonzalez-Garcia, D.G. Truhlar, J. Phys. Chem. A 109 (2005) 2012.
[43] Y. Zhao, D.G. Truhlar, J. Phys. Chem. A 109 (2005) 4209.